Quantum Mechanical and NMR Studies of Ring Puckering and *cis*/*trans*-Rotameric Interconversion in Prolines and Hydroxyprolines

Abil E. Aliev,* Simrath Bhandal, and Denis Courtier-Murias

Department of Chemistry, University College London, 20 Gordon Street, London WC1H 0AJ, United Kingdom

Received: June 26, 2009; Revised Manuscript Received: August 23, 2009

Nuclear magnetic resonance (NMR) and quantum mechanical (QM) studies have been carried out for proline (Pro) containing peptides: *N*-acetyl-L-proline (AcProOH) and *N*-acetyl-4-hydroxy-L-proline (AcHypOH). Preliminary results of variable temperature NMR measurements for Gly-Pro-Gly-Gly (GPGG), Val-Ala-Pro-Gly (VAPG), and Ala-Pro-Gly-Trp amide acetate salt (APGW) are also reported. The effect of solvent (D_2O, DMSO-d_6 and CD_3CN) on the pyrrolidine ring conformation and *cis*/*trans*-rotamerisation along the amide bond preceding Pro was investigated by temperature dependent NMR followed by detailed transition state (TS) searches for both conformational equilibria using QM methods. The results revealed the energetic characteristics of the TS, which were in satisfactory agreement with NMR, and the corresponding TS geometries, which are not available from experiment. The most remarkable feature of the *cis*/*trans*-rotamerisation is that the amide nitrogen in AcProOH and AcHypOH adopts a tetrahedral geometry in the TS. Various HF, DFT, and MP2 calculations together with implicit solvation modeling were employed in order to identify the most suitable QM protocols for reliable predictions of the geometry and the relative energies of the conformations of Pro and Hyp containing peptides in aqueous solution. Solution NMR results were used for the verification of the reliability of the QM predictions. The results indicate that the MP2 calculations combined with implicit solvation models are reasonably accurate in reproducing NMR measured populations of four different conformations of either AcProOH or AcHypOH in different solvents, whereas HF and DFT B3LYP calculations were significantly less accurate.

1. Introduction

Proline (Pro) is one of 20 natural amino acids with a distinctive cyclic side chain. Its specific conformational behavior is known to affect the denatured state of proteins by increasing the energy difference between the denatured and the native states.[1] There is no amide hydrogen in proline and the usual N−H···O type hydrogen bonds are not possible for Pro residues. In terms of other structural and functional aspects, proline can act as a structural disruptor in the middle of regular secondary structures such as α helices and β sheets. In transmembrane proteins, Pro residues are located in the middle of transmembrane helices and are highly conserved.[2] In water-soluble proteins, Pro residues in the center of α-helices can cause a kink of ≥20° of the long helix axis.[3]

Proline is one of the main building blocks in collagen, which is the main protein of connective tissue in mammals, consisting about 25% of the whole body protein content. Collagen consists of three peptide chains forming a triple-helix, with each chain consisting of about 1000 amino acid residues. Formation of the triple helix conformation requires the presence of a repeated -Gly-X-Y- sequence, the most common sequence being -Gly-Pro-Hyp- (Hyp = 4-hydroxy-L-proline), though other amino acid residues may also occur as X or Y. It is known that the five membered rings of Pro and Hyp stabilize the collagen triple helical structure.[4]

Compared with other natural amino acid residues, the peptide bond preceding Pro residues shows a higher tendency for the formation of the *cis*-rotamer (10−30% compared with 0.1% for other amino acid residues, Figure 1).[5] An important structural aspect of proline containing peptides is therefore the ratio and relative stability of *cis*- and *trans*-rotamers along the peptide bond preceding prolines.[6,7] In collagen, for example, all peptide bonds, including those of Pro and Hyp, are expected to be in the *trans*-conformation, and it is believed that high trans-to-cis ratios ensure higher stability of the triple helical structures. The trans-to-cis ratios have been used for the explanation of the stability of triple helical structures.[8−10]

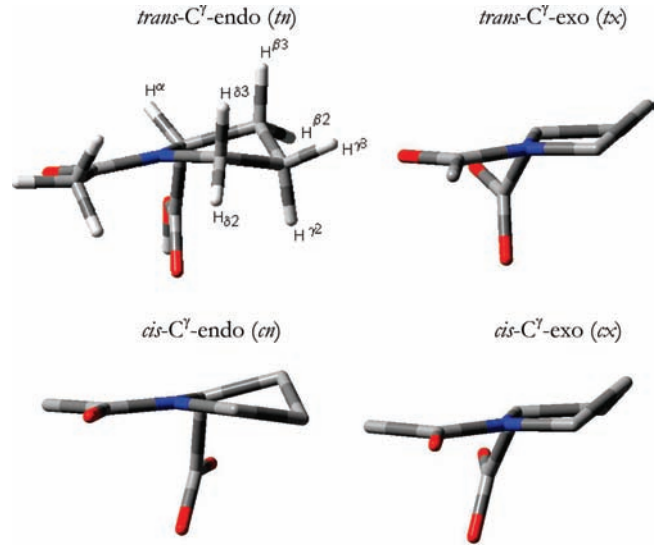

Figure 1. Four typical conformations of *N*-acetyl-L-proline.

Although proline is a relatively simple molecule, up to 20 different conformations are still possible for the pyrrolidine ring, which are separated by small energy barriers, thus making their

* Corresponding author. Phone: (+44) 020 7679 4616. Fax: (+44) 020 7679 7463. E-mail: a.e.aliev@ucl.ac.uk.

10.1021/jp906006w CCC: $40.75
Published on Web 09/16/2009

identification rather difficult.[11] An experimental approach most suitable for the solution state studies is NMR spectroscopy. The measurement of $^3J_{HH}$ couplings of the cyclic ring provides means for distinguishing various possible endo- or exo-conformations of the cyclic ring.[12,13] Variable temperature NMR can be used for estimating energy characteristics of the *cis*/*trans*-rotamerisation process. At the same time, the ring inversion process of the pyrrolidine ring is fast in the NMR time scale and only an averaged conformational behavior can be extracted from the dynamically averaged NMR parameters. In addition, the proline protons show strong coupling effects in ^{1}H NMR spectra requiring full line shape analysis.[13] Furthermore, a mixture of both *cis*- and *trans*-rotamers are observed in the same ^{1}H spectrum leading to further complication of the NMR spectra. While these problems can be addressed, a more fundamental problem with NMR is that on interpreting the measured averaged parameters there can be various possible models which equally well fit the observed data. Besides, while energy barriers can be measured from the variable temperature NMR measurements, establishing the structure of the transition state (TS) is beyond its capabilities. Quantum mechanical (QM) and molecular dynamics simulations (MD) are expected to be useful in this regard,[13−29] and herein we explore a combined NMR/QM approach for conformational studies of *N*-acetyl-L-proline (AcProOH) and *N*-acetyl-4-hydroxy-L-proline (AcHypOH).

2. Experimental Section

NMR Measurements and Calculations. AcProOH, AcHypOH, Gly-Pro-Gly-Gly (GPGG), Val-Ala-Pro-Gly (VAPG), and Ala-Pro-Gly-Trp amide acetate salt (APGW) were purchased from Sigma-Aldrich and were used without further purification. Solution ^{1}H NMR spectra were recorded on Bruker NMR spectrometers AVANCE400, AVANCE500, and AVANCE600 equipped with a Bruker 5 mm cryoprobe (600 MHz) or room temperature probes (400 and 500 MHz). Data acquisition and processing were performed using standard Bruker TopSpin (version 2.1) software. ^{1}H and ^{13}C chemical shifts in D_2O were calibrated using sodium 3-(trimethylsilyl)propionate (TSP, ^{1}H 0 ppm) and dioxane (^{1}H 3.75 ppm, ^{13}C 67.19 ppm). The populations of *trans*- and *cis*-rotamers (in %) were measured by integration of ^{1}H NMR spectra. The standard deviation of such measurements was found to be better than 1%. For example, from the integrations of 45 ^{1}H spectra measured for AcProOH in D_2O at 298 K at three different ^{1}H frequencies (400, 500, and 600 MHz) the standard deviation was estimated as 0.44%. The populations of C^γ-exo and C^γ-endo conformers for each of the rotamers were determined by the analysis of the measured vicinal spin−spin couplings using simulated annealing, as described previously,[13] with the estimated least-squares fitting errors included in Table 1. High temperature NMR measurements were calibrated using ethylene glycol. The coalescence temperatures were measured using intervals of 1° around the coalescence point and at least 10 min were waited between experiments to allow the system to achieve the equilibrium at each temperature.

Iterative full line shape analyses were carried out using *g*NMR.[30] Least-squares fittings of the vicinal ^3J-couplings were carried out using a Fortran program based on an approach described previously,[12,13] but using a simulated annealing algorithm,[31] and Karplus-type equations as described by Haasnoot et al.[32] (listed as 8B, 8C, and 8D in ref 32).

Computational Details. All quantum mechanical calculations were carried out using *Gaussian 03*.[33] Geometry optimisations were done using mainly HF/6-31+G(d), MP2/6-31+G(d), and MP2/cc-pVDZ levels of theory; however, other levels were also tested (see Results and Discussion). Water solvent effects were introduced in the quantum mechanical calculations using the reaction field methods IEFPCM[34] and CPCM[35] models, as implemented in *Gaussian 03*. Additional frequency calculations were also undertaken in order to verify that the optimized geometries correspond to true minima or transition states by checking whether no or one imaginary frequency was encountered. These calculations were also used for computations of enthalpies and Gibbs free energies at 298 K and 1 atm, as well as at coalescence temperatures at 1 atm for better comparison of the NMR and QM results.

TABLE 1: Conformational Characteristics Obtained from the Simulated Annealing Fittings of ^3J-Couplings at 298 K[a]

compound	rotamer	solvent	P^{endo}/P^{exo}(°)	χ_m(°)	x^{endo}	rms (Hz)
AcProOH	*trans*	CD_3CN	184/20	41.9	0.708	0.56
	trans	DMSO-d_6	183/22	41.0	0.659	0.53
	trans	D_2O	185/14	40.3	0.613	0.49
	cis	CD_3CN	178/31	40.9	0.786	0.61
	cis	DMSO-d_6	179/33	40.8	0.784	0.56
	cis	D_2O	180/23	40.1	0.795	0.55
AcHypOH	*trans*	CD_3CN	209/13	43.4	0.286	0.31
	trans	DMSO-d_6	210/12	43.2	0.251	0.33
	trans	D_2O	203/13	41.6	0.103	0.39
	cis	CD_3CN	195/20	41.7	0.296	0.36
	cis	DMSO-d_6	192/19	41.5	0.322	0.36
	cis	D_2O	188/22	40.9	0.198	0.42
GPGG	*trans*	D_2O	189/11	41.0	0.543	0.49
	cis	D_2O	181/24	41.1	0.799	0.66
VAPG	*trans*	D_2O	187/14	41.0	0.523	0.47
	cis	D_2O	177/20	42.1	0.826	0.59

[a] The value of χ_m is assumed to be the same in both endo- and exo-conformations. The estimated least-squares fitting errors were ±1.0° for *P*, ±0.3° for χ_m, and ±0.003 for x^{endo}.

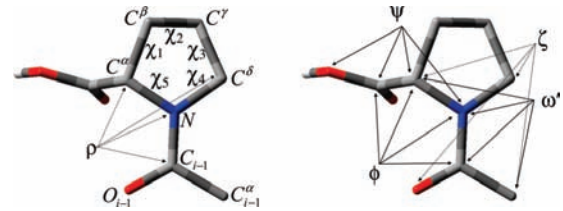

Figure 2. Atom labeling and definition of endocyclic (left) and exocyclic (right) torsional angles for AcProOH. The angles ρ and ζ are defined as $N-C^\alpha_{i-1}-C^\alpha-C^\delta$ and $C^\alpha_{i-1}-O_{i-1}-C^\delta-C^\alpha$, respectively.

Conformational Notation. We use the original conformational notation proposed by Haasnoot et al. for L-prolines.[12] In particular, E and T letters are used to denote envelope and twist conformations, with a superscript (subscript) indicating a proline ring atom above (below) the ring (see Table 1 of ref 12). The downward orientation of the CO_2 group is used as a reference view and the exo- and endo-orientations of the ring carbons are defined relative to CO_2 (Figure 1). The definition of endo- and exocyclic torsional angles is shown in Figure 2.

For the ring conformational equilibrium in either *cis*- or *trans*-rotamer, a two-site exchange model between C^γ-endo and C^γ-exo conformations was assumed based on the previous NMR and MD results.[13] The populations of these ring conformations in each rotamer are denoted as x^{endo} and x^{exo} ($x^{endo} + x^{exo} = 1$).[12,13]

The pseudorotation phase angle, *P*, which identifies a given conformation on the pseudorotation circle,[11] and the pseudorotation amplitude χ_m, which is the maximum value attained by $\chi_1-\chi_5$.[12] The calculations of *P* and χ_m were done using equations by Westhof-Sundaralingam:[36]

$$P = \tan^{-1}\left(\frac{B}{A}\right) \text{ and } \chi_m = (A^2 + B^2)^{1/2},$$

where

$$A = \frac{2}{5}\sum_{i=1}^{5}\chi_i \cos\left(\frac{4\pi}{5}(i-2)\right) \text{ and}$$

$$B = -\frac{2}{5}\sum_{i=1}^{5}\chi_i \sin\left(\frac{4\pi}{5}(i-2)\right)$$

Note that 180° is added to the calculated P value if $\chi_2 < 0$.

3. Results and Discussion

NMR Analysis. Upon recording the NMR spectra of AcProOH at room temperature, the presence of two rotamers can be identified, with the *cis*-rotamer as the less populated form. When in DMSO-d_6, the population of *trans*-rotamer is 72%, while in CD_3CN it is slightly higher at 82%. In D_2O, the population of *trans*-rotamer is 79%, which corresponds to the free energy difference (ΔG) of 3.3 kJ mol^{-1} for the *cis*-rotamer relative to the *trans*-rotamer. For AcProNHMe and AcProNH_2 in D_2O, the population of *trans*-rotamer is 76% ($\Delta G = 2.9$ kJ mol^{-1})[37] and 75% ($\Delta G = 2.7$ kJ mol^{-1}).[38] For AcProNHMe in DMSO-d_6 the population of *trans*-rotamer is 65%, while in CD_3CN it is 80%. From these results, the relative content of the *trans*-rotamer in AcProOH is slightly higher than that of AcProNHMe in all three solvents used.

The ^{1}H spectra of the Pro fragment were characteristic of strongly coupled spin systems and were analyzed numerically using full line shape analysis. The measured NMR parameters are included in Supporting Information (Table S1−S16). Conformational characteristics were determined by the analysis of the measured vicinal spin−spin couplings using simulated annealing, as described previously.[13]

The ring geometries of *cis*- and *trans*-AcProOH were found to be essentially the same in CD_3CN, DMSO-d_6 and D_2O (Table 1), while a significant change in the predicted geometry was found for *cis*- and *trans*-AcHypOH in D_2O compared with AcHypOH in DMSO-d_6 or CD_3CN. As discussed below, the NMR predicted values of P and χ_m (Table 1) were supported by those calculated by the MP2, DFT, and HF methods in aqueous solutions, with a better agreement observed for *trans*-rotamer compared with *cis*-rotamer. From the comparison of the pseudorotation parameters of the pyrrolidine ring in AcProOH, GPGG, and VAPG in both *cis*- and *trans*-rotamers in D_2O (Table 1), the neighboring residues have no significant effect on the geometry of the pyrrolidine ring. However, a decrease of the population of the C^γ-endo conformer (x^{endo}, Table 1) was observed in *trans*-GPGG and *trans*-VAPG compared with *trans*-AcProOH.

Relative Stability of *cis*- and *trans*-Rotamers. The rotameric cis-to-trans ratio, which is equal to the equilibrium constant K, was found to vary with temperature. By fitting ln(K) versus 1/T, the enthalpy (ΔH) and entropy (ΔS) changes can be calculated using

$$K = \frac{p_{cis}}{p_{trans}}$$

$$\Delta G = -RT\ln(K) = \Delta H - T\Delta S$$

$$\ln(K) = -\frac{\Delta H}{R}\frac{1}{T} + \frac{\Delta S}{R}$$

where p_{cis} and p_{trans} are populations of *cis*- and *trans*-rotamers, respectively, T is the temperature (in K), R is the universal gas constant, and ΔG is the change in the standard Gibbs free energy. Values for ΔH and ΔS obtained from the least-squares fitting are shown in Table 2. In order to study the dependence of the *cis*-to-*trans* ratio on the nature of the residue preceding the Pro residue, we have included the thermodynamic characteristics measured for Gly-Pro-Gly-Gly (GPGG) and Val-Ala-Pro-Gly (VAPG), together with the ΔG value at 298 K (ΔG(298 K)) for Ala-Pro-Gly-Trp amide acetate salt (APGW).

Although only a small number of peptides has been analyzed so far, some interesting conclusions can be derived from the results presented in Table 2: (i) The stability of the Hyp residue toward the trans-to-cis rotamerisation is significantly higher than that of Pro. (ii) Compared with DMSO-d_6 and CD_3CN, an aqueous environment increases the enthalpic stability of Pro and Hyp residues toward the trans-to-cis rotamerisation process. (iii) For the Pro containing peptides AcProOH, GPGG, VAPG, and APGW in D_2O, the increase of the size of the residue preceding the Pro residue leads to an increase of ΔH, while the change of ΔG is less well-defined.

In collagen, where each peptide chain consists of approximately 1000 amino acid residues, all peptide bonds are in *trans*-conformation. From our preliminary results, it can be speculated that the enthalpic stability of the Pro residues near the *N*-termini of collagen chains toward the trans-to-cis rotamerisation process may be less than those near the C-termini or in the middle of the chain, and the thermal denaturation of collagen may therefore prefer to start at its *N*-termini. Further examples of Pro peptides with varying size of the peptide chain are currently under investigation in order to verify this possibility.

Energy Barriers of *cis*/*trans*-Rotamerisation from NMR. The coalescence temperature (T_c) measurements were undertaken in order to determine the free energy of activation, which are summarized in Table 3. The free energy barriers were determined using the method described by Shanan-Atidi and Bar-Eli.[39] The results show a significant decrease of the $\Delta G^\ddagger$ values (up to ca. 7%) on changing the solvent from D_2O to DMSO-d_6, which can be attributed to hydrogen bonding of one or more water molecules to the carbonyl oxygen of the acetyl group. A similar explanation was provided for *N*-methylacetamide based on ab initio results,[40] according to which hydrogen bonding of the carbonyl oxygen to water may increase the barrier to cis/trans rotameric exchange by up to 8.8 kJ mol^{-1}. From the comparison of the data presented in Table 3 for AcProOH, GPGG, and VAPG in D_2O, a decrease of the $\Delta G^\ddagger$ values is also observed on increasing the size of the residue preceding the Pro residue. This observation is in agreement with the previous findings for the amide bond rotation.[41]

Comparison of QM and NMR Results. We first compare the results of geometry predictions by various QM methods and basis set levels (Table 4). The differences in the geometries predicted by HF, B3LYP, MP2, CCD, and CCSD are not significant, although the ring puckering (reflected in the χ_m value) is less pronounced in the case of the HF geometries. The QM calculated geometries for the *trans*-conformers were in satisfactory agreement with the NMR measurements, whereas some significant differences were found for *cis*-conformers. However, the accuracy of geometry predictions by NMR is

TABLE 2: Values of ΔH, ΔS, and ΔG(298 K) Measured from Variable Temperature ^{1}H NMR Spectra for the *cis*/*trans*-Rotameric Exchange

peptide	substituent R preceding Pro(Hyp)-CO	solvent	ΔH (kJ mol^{-1})	ΔS (J K^{-1} mol^{-1})	ΔG(298 K) (kJ mol^{-1})
AcProOH	-CH_3	D_2O	3.3 ± 0.1	0.2 ± 0.2	3.2 ± 0.1
AcProOH	-CH_3	DMSO-d_6	2.9 ± 0.1	2.1 ± 0.3	2.3 ± 0.1
AcProOH	-CH_3	CD_3CN	−0.7 ± 0.1	−15.0 ± 0.2	3.8 ± 0.1
GPGG	-Gly	D_2O	4.9 ± 0.3	1.2 ± 0.8	4.5 ± 0.3
VAPG	-Ala-Val	D_2O	6.7 ± 0.6	7.2 ± 1.8	4.4 ± 0.6
APGW	-Ala	D_2O	-	-	5.2 ± 0.2
AcHypOH	CH_3	D_2O	4.4 ± 0.2	1.9 ± 0.5	3.8 ± 0.2
AcHypOH	CH_3	DMSO-d_6	4.4 ± 0.2	5.2 ± 0.8	2.9 ± 0.2
AcHypOH	CH_3	CD_3CN	1.9 ± 0.1	−9.3 ± 0.2	4.7 ± 0.1

TABLE 3: Free Energies of Activation for trans → cis ($\Delta G^{\ddagger}_{tc}$) and cis → trans ($\Delta G^{\ddagger}_{ct}$) Rotamerisations at the Coalescence Temperatures Shown

peptide	solvent	T_c (K)	$\Delta G^{\ddagger}_{ct}$(kJ mol^{-1})	$\Delta G^{\ddagger}_{tc}$(kJ mol^{-1})
AcProOH	D_2O	404	82.5	88.8
AcProOH	DMSO-d_6	388	78.3	80.5
GPGG	D_2O	380	79.9	84.5
GPGG	DMSO-d_6	357	72.5	75.3
VAPG	D_2O	372	76.6	80.5
VAPG	DMSO-d_6	342	70.4	74.3
AcHypOH	D_2O	402	84.7	88.3
AcHypOH	DMSO-d_6	380	79.6	82.1

TABLE 4: Pseudorotation Parameters P (°)/χ_m (°) of AcProOH in the Gas Phase and in Water (IEFPCM)

method	*tn*	*tx*	*cn*	*cx*
NMR (in D_2O)	185/40.3	14/40.3	180/40.1	23/40.1
CCSD/cc-pVDZ (gas phase)	171/38.8	23/39.4	168/39.6	16/39.1
CCD/cc-pVDZ (gas phase)	171/38.7	23/39.3	168/39.5	16/39.0
MP2/cc-pVTZ (gas phase)	176/39.8	17/40.5	172/39.8	13/40.3
MP2/cc-pVDZ (gas phase)	174/39.9	20/40.5	170/40.6	13/40.4
MP2/6-31+G(d) (gas phase)	174/39.0	21/40.3	172/39.6	17/40.1
HF/6-31+G(d) (gas phase)	174/36.1	21/37.3	171/37.0	20/37.4
CCSD/cc-pVDZ (in water)	184/39.0	10/39.5	170/40.0	17/39.4
MP2/cc-pVDZ (in water)	180/40.3	10/40.8	171/40.8	14/40.7
MP2/6-31+G(d) (in water)	181/39.0	13/40.4	173/39.4	17/40.3
B3LYP/6-31G(d) (in water)	179/37.1	11/37.8	172/37.5	17/37.5
B3LYP/6-31+G(d) (in water)	181/36.0	12/37.7	173/36.9	17/37.6
HF/cc-pVDZ (in water)	181/36.4	13/37.7	172/37.1	19/37.6
HF/6-31+G(d) (in water)	180/36.5	13/37.8	172/37.1	19/37.7
HF/4−31G (in water)	182/36.9	16/37.0	170/37.2	24/36.9

subject to systematic errors (e.g., from the parametrization of the Karplus type relationships). From this point of view, the differences of less than 10° in P values between NMR and QM predictions can be considered as satisfactory.

While conventional HF and DFT methods are known to be accurate in predicting molecular geometries, their performance in predicting energetic characteristics is usually less satisfactory.[42−46] We have therefore undertaken several sets of calculations in order to identify the level of theory suitable for accurate predictions of the relative stability of Pro and Hyp conformers.

TABLE 5: Populations of Conformers (in %) in AcProOH and AcHypOH in Water at 298 K[a]

method	*cn*	*cx*	*tn*	*tx*	rms(%)
Ac-Pro−OH					
NMR	17	4	48	31	
MP2/6-31++G(2d,2p)//MP2/6-31+G(d)	14	3	45	39	4
MP2/aug-cc-pVDZ//MP2/cc-pVDZ	18	9	42	31	4
MP2/6-31+G(d)	15	3	51	31	2
MP2/6-31+G(d) (CPCM)	12	3	59	26	6
MP2/cc-pVDZ	23	5	51	21	6
MP2/cc-pVDZ (CPCM)	23	5	51	21	6
HF/6-31+G(d)	6	2	64	28	10
HF/cc-pVDZ	9	2	66	23	10
HF/4−31G	8	1	73	17	15
B3LYP/6-31+G(d)	6	6	43	45	10
B3LYP/6-31G(d)	16	6	64	14	12
B3LYP/cc-pVDZ	19	7	46	28	3
Ac-Hyp−OH					
NMR	3	14	9	74	
MP2/6-31++G(2d,2p)//MP2/6-31+G(d)	1	12	6	81	4
MP2/aug-cc-pVDZ//MP2/cc-pVDZ	2	40	4	54	16
MP2/6-31+G(d)	1	10	6	83	5
MP2/6-31+G(d) (CPCM)	2	9	6	83	5
MP2/cc-pVDZ	5	15	14	66	5
MP2/cc-pVDZ (CPCM)	4	15	13	68	4
HF/6-31+G(d)	4	2	41	53	20
HF/cc-pVDZ	5	6	43	46	22
B3LYP/6-31+G(d)	12	26	7	55	12
B3LYP/6-31G(d)	8	9	28	54	14
B3LYP/cc-pVDZ	9	14	35	43	20

[a] Unless otherwise specified, the IEFPCM solvation model was used.

In Table 5, we compare populations of conformers in AcProOH and AcHypOH obtained by NMR, HF, DFT, and MP2 methods in water using IEFPCM and CPCM solvation models. In Table 6, we compare the results of MP2 calculations in DMSO and CH_3CN solutions using IEFPCM and CPCM solvation models. The geometries of all four conformers were optimized at the shown levels of theory. The values of the sum of electronic and thermal free energies from the subsequent frequency calculations were used for calculating populations of conformers. The rms values calculated over four values of conformer populations were used as a measure of agreement between NMR and QM levels of theory.

From the results presented in Table 5, HF and DFT methods fail to satisfactorily predict populations of conformers in water, whereas MP2 shows surprisingly good agreement with the experimental results in different solvents (Tables 5 and 6). We have also used "mixed" MP2 calculations where larger basis sets (6-31++G(2d,2p) and aug-cc-pVDZ) were used at the frequency calculations stage using optimized geometries from MP2/6-31+G(d) and MP2/cc-pVDZ. However, as apparent from the results for AcProOH and AcHypOH (Table 5), the performance of these mixed level calculations is somewhat unpredict-

TABLE 6: Populations of Conformers (in %) in AcProOH and AcHypOH in Different Solvents at 298 K Predicted by NMR and MP2 Methods

method	solvent	*cn*	*cx*	*tn*	*tx*	rms (%)
Ac-Pro−OH						
NMR	DMSO-d_6	22	6	48	24	
MP2/6-31+G(d) (IEFPCM)	DMSO	12	3	56	29	7
MP2/6-31+G(d) (CPCM)	DMSO	13	4	55	29	6
MP2/cc-pVDZ (IEFPCM)	DMSO	22	5	52	22	2
MP2/cc-pVDZ (CPCM)	DMSO	22	5	51	22	2
NMR	CD_3CN	14	4	58	24	
MP2/6-31+G(d) (IEFPCM)	CH_3CN	12	3	54	31	4
MP2/6-31+G(d) (CPCM)	CH_3CN	15	4	49	32	6
MP2/cc-pVDZ (IEFPCM)	CH_3CN	22	4	54	20	5
MP2/cc-pVDZ (CPCM)	CH_3CN	22	4	54	20	5
Ac-Hyp−OH						
NMR	DMSO-d_6	4	9	22	65	
MP2/6-31+G(d) (IEFPCM)	DMSO	2	10	6	82	12
MP2/6-31+G(d) (CPCM)	DMSO	2	9	7	82	11
MP2/cc-pVDZ (IEFPCM)	DMSO	5	19	23	53	8
MP2/cc-pVDZ (CPCM)	DMSO	5	15	18	62	4
NMR	CD_3CN	5	19	22	54	
MP2/6-31+G(d) (IEFPCM)	CH_3CN	2	11	8	79	15
MP2/6-31+G(d) (CPCM)	CH_3CN	2	7	7	84	18
MP2/cc-pVDZ (IEFPCM)	CH_3CN	4	18	16	62	5
MP2/cc-pVDZ (CPCM)	CH_3CN	5	17	16	62	5

able. Attempts were also made to optimize geometries at MP2/6-31++G(2d,2p) and MP2/aug-cc-pVTZ levels; however, these proved to be prohibitively expensive. Considering the overall performance, we can conclude that the MP2 calculations combined with either IEFPCM or CPCM solvation models are reasonably accurate in reproducing NMR measured conformational characteristics of either AcProOH or AcHypOH, whereas HF and DFT B3LYP calculations are significantly less accurate. As the IEFPCM model performed slightly better than the CPCM model for the MP2 calculations in water (Table 5), only the IEFPCM model is used in the transition state searches in water described below.

QM Analysis of the Pseudorotation of the Pyrrolidine Ring. The calculated thermodynamic properties are summarized in Table 7, where ΔE is defined as the difference in sum of electronic and zero point (ZP) energies. Similarly, ΔH is equal to the difference in the sum of electronic and thermal enthalpies, whereas ΔG corresponds to the difference in the sum of electronic and thermal free energies.

The $\Delta E^{\ddagger}$ values are comparable to those determined for AcProNHMe in water.[22,23] However, in AcProOH, the C^{γ}-endo conformer was established as the minimum energy conformer in agreement with the NMR results (see below discussion), whereas the C^{γ}-exo-conformer was reported as the preferred conformation in AcProNHMe according to the B3LYP/6-311++G(d,p)//HF/6-31+G(d) calculations in water using the CPCM solvation model.[22,23]

From the MP2/6-31+G(d) calculations for AcHypOH, the $\Delta E^{\ddagger}$, $\Delta H^{\ddagger}$, and $\Delta G^{\ddagger}$(298 K) values for the *trans*-TS relative to the lowest energy *tx* conformer were 14.9, 12.8, and 17.9 kJ mol^{-1} in water and 9.3, 6.9, and 13.0 kJ mol^{-1} in the gas phase (Supporting Information, Table S17). These results suggest that the pyrrolidine ring in AcHypOH is less flexible than in AcProOH in aqueous environment.

The geometric characteristics of different conformers and transition states are compared in Table 8. The improper dihedral angle $\rho(N-C_{i-1}-C^{\alpha}-C^{\delta})$ is introduced in order to reflect the pyramidality of the N atom in Pro. Some significant differences in the torsion angles for the *tn* and *tx* ground state conformations, as well as for transition state (TS) at the MP2/cc-pVDZ level and HF/6-31+G(d) levels, were found. As apparent from Table 8, in the ground state, the N atom of Pro is not exactly planar, especially in the gas phase on using MP2 calculations. However, this is not a specific feature characteristic for the Pro nitrogen. For comparison, in the case of MP2/cc-pVDZ optimized geometries of dimethylacetamide ρ equals 10.8° in the gas phase and 7.0° in water (IEFPCM solvation model). Additional MP2/aug-cc-pVTZ and CCSD/cc-pVDZ calculations of the *tn* conformer of AcProOH in the gas phase also showed a slightly out of plane N atom with ρ equal 9° and 10°, respectively. Overall, the Pro ring and the Pro nitrogen geometries predicted by MP2/cc-pVDZ and MP2/6-31+G(d) (Supporting Information, Table S18) are less planar in both ground and transition states than those by HF/6-31+G(d).

All of the transition states between C^{γ}-endo and C^{γ}-exo ring conformations for AcProOH (Table 8) and AcHypOH (see below) were found to have an ^{N}E geometry (Figure 3). A similar ^{N}E ($P = 94°$, $\chi_m = 28.4°$) transition state geometry was previously reported for the ring flip process in the *trans*-rotamer of AcProNHMe based on the B3LYP/6-311++G(d,p) calculations.[20] The planarity of the N atom is significantly distorted in the transition state with $\rho \approx 18°$. However, the $N-C_{i-1}$ bond in AcProOH was only slightly longer in the TS compared with the ground states; for example, from MP2/cc-pVDZ calculations in water, the $N-C_{i-1}$ bond lengths were 1.363 Å (in *tn*) and 1.371 Å (in TS(*tn* ↔ *tx*)).

From the calculated maximum puckering angle χ_m, it is clear that $\Delta G^{\ddagger}$(298 K) (Table 7) is dependent on χ_m values in both the ground and the transition states (Table 8). In particular, at the MP2 level, χ_m is greater than that at the HF level in *tn* and *tx* conformers. Correspondingly, the energy barrier for the conformational ring interconversion is larger. The smaller value of the $\Delta G^{\ddagger}$(298 K) at the HF level may also be attributed to the fact that the TS geometry by HF/6-31+G(d) is more flattened than that by MP2/cc-pVDZ (Table 8).

QM Analysis of cis/trans Rotameric Interconversion. Initially, synchronous transit-guided quasi-Newton (STQN) method was used for the transition state searches.[47] Here the trans, cis, and an initial transition state structures were provided as input data. The initial TS structure was built by the rotation about the $N-C_{i-1}$ bond by 90°. Results obtained by this method were not satisfactory, as the energy differences between the values for the TS and those for the *tn*-conformer in water were approximately 160 kJ mol^{-1} by HF/6-31+G(d) and approximately 130 kJ mol^{-1} by MP2/cc-pVDZ, which are significantly higher than the experimentally measured value of approximately 88 kJ mol^{-1}.

Subsequent HF and MP2 calculations were carried out in which the amide bond rotamerisation was simulated in a stepwise manner. As shown previously, the virtual angle ζ (Figure 2) is better suited for describing the progress of the rotamerisation process than ω'.[16] The dihedral angle ζ was either incremented or decremented in 10° steps in order to simulate clockwise or anticlockwise rotation of the acetyl fragment. At each step, the dihedral angle ζ was fixed with all of the remaining degrees of freedom optimized using MP2 calculations. A relaxed one-dimensional (1D) potential energy surface (PES) scan was performed in this manner, and minimized energies at each step were obtained (Figure 4).

This method provides the following $\Delta E^{\ddagger}$ values for the trans-to-cis rotameric conversion on anticlockwise rotation for C^{γ}-endo and C^{γ}-exo conformers of AcProOH in water: $\Delta E^{\ddagger} = 87.6$ kJ mol^{-1} and 86.5 kJ mol^{-1}, respectively, at the MP2/6-31+G(d)

TABLE 7: Energetic Characteristics (kJ mol^{-1}) of the endo/exo TS for AcProOH[a]

	HF/6-31+G(d)			MP2/cc-pVDZ			MP2/6-31+G(d)		
Conformer	$\Delta E^{\ddagger}$	$\Delta H^{\ddagger}$	$\Delta G^{\ddagger}$(298 K)	$\Delta E^{\ddagger}$	$\Delta H^{\ddagger}$	$\Delta G^{\ddagger}$(298 K)	$\Delta E^{\ddagger}$	$\Delta H^{\ddagger}$	$\Delta G^{\ddagger}$(298 K)
TS(*tn*↔*tx*) (H_2O)	10.6	9.2	11.5	12.3	10.6	14.6	12.9	11.3	14.5
TS(*tn*↔*tx*) (gas)	8.5	6.8	10.5	10.1	8.3	12.5	9.9	8.1	11.9
TS(*cn*↔*cx*) (H_2O)	10.2	8.7	11.5	11.5	9.6	14.1	12.3	10.6	14.4
TS(*cn*↔*cx*) (gas)	9.5	7.8	11.3	10.5	8.5	14.1	10.8	8.9	14.0

[a] The TS energies are given with respect to the C^{γ}-endo conformer with the lowest energy.

TABLE 8: Torsion Angles (°) and Pseudorotation Parameters (°) for *trans*-AcProOH from QM Calculations[a]

	MP2/cc-pVDZ						HF/6-31+G(d)					
Conformer	ω'	ϕ	ψ	χ_m	P	ρ	ω'	ϕ	ψ	χ_m	P	ρ
tn (H_2O)	178	−67	158	40	180	5	−178	−73	161	36	180	−1
tx (H_2O)	180	−58	146	41	11	−1	−178	−63	154	38	13	−4
cn (H_2O)	−6	−72	171	41	171	6	2	−81	171	37	172	−2
cx (H_2O)	−2	−62	166	41	14	−1	−2	−65	167	38	19	−2
TS(*tn*↔*tx*) (H_2O)	170	−68	168	34	93	17	177	−73	164	25	92	7
TS(*cn*↔*cx*) (H_2O)	−22	−67	−179	36	90	19	−10	−76	173	28	89	7
TS(*tn*↔*cn*) (H_2O)	116	−77	174	49	257	−39						
TS(*tx*↔*cn*) (H_2O)	116	−78	175	49	256	−39						
tn (gas)	174	−63	155	40	173	10	178	−72	158	36	173	3
tx (gas)	176	−54	143	41	19	6	178	−62	152	37	21	1
cn (gas)	−8	−70	169	41	169	8	1	−78	169	37	171	0
cx (gas)	1	−62	165	40	13	−2	−1	−64	167	37	20	−1
TS(*tn*↔*tx*) (gas)	168	−65	165	36	92	20	173	−70	162	30	89	12
TS(*cn*↔*cx*) (gas)	−24	−65	179	37	90	21	−12	−73	171	30	88	10

[a] The improper dihedral angle ρ(N−C_{i-1}-C^{α}-C^{δ}) is introduced in order to reflect the pyramidality of the N atom in Pro. The dihedral angle Ψ is defined as HO-C_i-C^{α}-N.

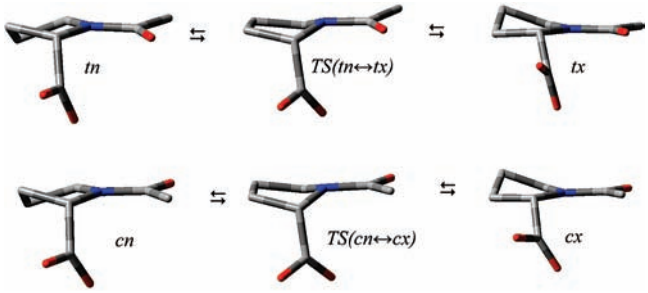

Figure 3. Geometries of the ground and transition state conformations of AcProOH optimized at the MP2/cc-pVDZ level in water using the IEFPCM solvation model.

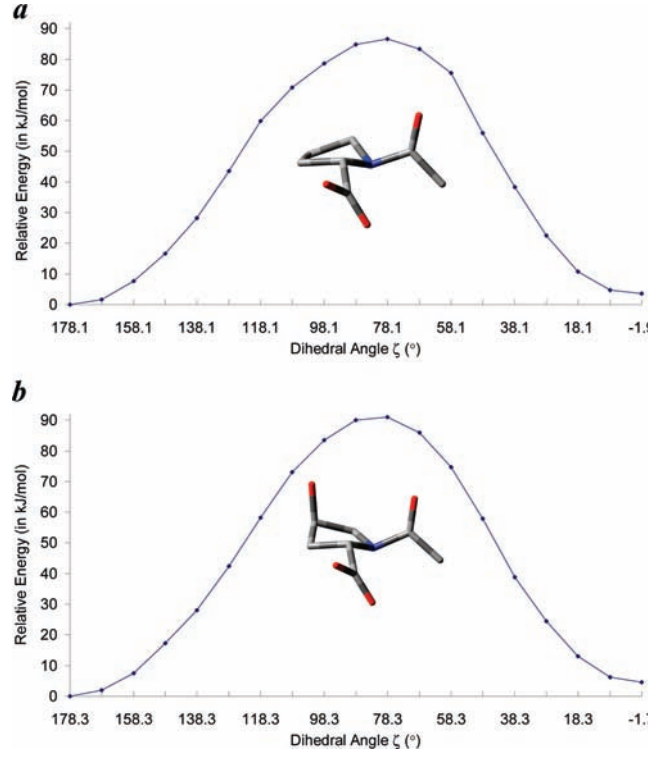

Figure 4. Anticlockwise rotations starting from the *tx* conformations of AcProOH (a) and AcHypOH (b) in water by MP2/6-31+G(d) using the IEFPCM solvation model. The highest energy structures are also shown. The change of the ring conformation from $P = -88°/\chi_m = 49.1°$ at $\zeta = 98.1°$ to $P = 268°/\chi_m = 49.2°$ at $\zeta = 88.1°$ was observed for AcProOH (a). No such transition was observed for AcHypOH.

level and 87.5 kJ mol^{-1} and 87.0 kJ mol^{-1}, respectively, at the MP2/cc-pVDZ level. We note that significantly lower values in the wide range of 54.8−80.7 kJ mol^{-1} for the barriers to rotation of the Ac-Pro peptide bond in AcProNHMe were reported previously on the basis of the calculation at the HF/6-31+G(d) level with the CPCM solvation model.[19] In a subsequent publication by the same group, the new value of $\Delta G^{\ddagger}_{tc}$(298 K) = 90.4 kJ mol^{-1} in water was reported on the basis of the B3LYP/6-311++G(d,p)//CPCM HF/6-31+G(d) calculations for the trans-to-cis rotameric conversion.[22] No MP2 transition state searches were reported for AcProNHMe.

As apparent from the highest energy structures shown in Figure 4, nitrogen adopts a tetrahedral geometry near the transition state ($P = 255°$, $\chi_m = 48.5°$, $\rho = -37.3°$ for AcProOH shown in Figure 4a and $P = -28°$, $\chi_m = 43.9°$, $\rho = -33.8°$ for AcHypOH shown in Figure 4b). Interestingly, the anticlockwise rotation starting from the *tx* conformation of AcProOH leads to the highest energy structure with the *endo*-conformation of the ring (Figure 4), similar to that found on the anticlockwise rotation starting from the *tn* conformation. Consequently, both cases lead to the final structure in the *cn* conformation, which has a lower relative energy compared with the *cx* conformation according to the NMR results (Table 1). No such ring transition was found for the *tn* conformation of AcHypOH, presumably

TABLE 9: Free Energies of Activation (in kJ mol^{-1}) for trans → cis Rotamerisation in Water

method	temperature, K	$\Delta G^{\ddagger}_{tcn}$ (kJ mol^{-1})[a]	$\Delta G^{\ddagger}_{tcx}$ (kJ mol^{-1})[a]	$\Delta G^{\ddagger}_{tc}$ (kJ mol^{-1})[a]
Ac-Pro−OH				
MP2/6-31+G(d)	298	86.2	85.9	
MP2/cc-pVDZ	298	77.2	75.0	
MP2/6-31+G(d)	404	88.1	86.9	87.6
MP2/cc-pVDZ	404	78.3	76.2	77.7
NMR	404			88.8
Ac-Hyp−OH				
MP2/6-31+G(d)	298	84.7	91.1	
MP2/cc-pVDZ	298	76.6	74.9	
MP2/6-31+G(d)	402	85.9	92.7	92.2
MP2/cc-pVDZ	402	77.0	80.4	79.8
NMR	402			88.3

[a] Free energy barriers were determined as a difference in Gibbs free energies in water: $\Delta G^{\ddagger}_{tcn} = \Delta G_{TS} - \Delta G_{tn}$ and $\Delta G^{\ddagger}_{tcx} = \Delta G_{TS} - \Delta G_{tx}$ (*tcn* and *tcx* denote trans-to-cis rotamerisation in C$^{\gamma}$-endo and C$^{\gamma}$-exo conformations, respectively). [b] For QM calculations: $\Delta G^{\ddagger}_{tc} = x^{\text{endo}}\,\Delta G^{\ddagger}_{tcn} + (1\text{-}x^{\text{endo}})\Delta G^{\ddagger}_{tcx}$.

because of the higher free energy barrier for the endo/exo transition in AcHypOH compared with that in AcProOH (17.9 and 14.5 kJ mol^{-1}, respectively, at 298 K from MP2/6-31+G(d) IEFPCM(H_2O) calculations).

Having identified the structure near the TS, we then used the structure with the highest energy from the torsional scans as the third structure in the new set of STQN searches. Additional frequency calculations were undertaken in order to confirm that the optimized structure corresponds to the TS. The final TS geometries for AcProOH are included in Table 8 and in Supporting Information (Table S18). In a similar manner, we have also located the transition states for AcHypOH, details of which are included in Supporting Information (Table S19).

From the MP2/cc-pVDZ calculations in water, the angle ρ reflecting the pyramidality of the N atom reaches a value of −38.7°. For comparison, calculations at the same level in water predict ρ = 35.2° and the N−C bond length of 1.459 Å in trimethylamine (34.5° and 1.456 Å, respectively, in the gas phase), the N atom of which is expected to be pyramidal. The N−C_{i-1} bond in AcProOH was significantly longer in the TS compared with that in the ground states; for example, from MP2/cc-pVDZ calculations in water, the N−C_{i-1} bond lengths were 1.363 Å (in *tn*) and 1.460 Å (in TS(*tn* ↔ *cn*)). These MP2 results are in agreement with those reported recently for AcProNHMe in water by QM/MM MD simulations, in which HF/4−31G level of theory was used for AcProNHMe.[29]

In Table 9, we compare the MP2 calculated energy barriers for trans-to-cis rotameric conversion determined as a difference in Gibbs free energies, which were calculated using frequency calculations at 298 K. Additional high-temperature calculations were also undertaken for better comparison with the NMR data. The MP2/6-31+G(d) results for both AcProOH and AcHypOH at the corresponding coalescence temperatures are in good agreement with the experimentally determined values. As discussed above, compared with HF and DFT methods, the MP2/6-31+G(d) protocol combined with the IEFPCM solvation model is also better suited for reproducing other conformational characteristics in aqueous solutions than MP2/cc-pVDZ, such as NMR measured populations and geometries of four different conformations of either AcProOH or AcHypOH.

In conclusion, our results reveal that the ground and transition states with the energetic characteristics in satisfactory agreement with NMR can be obtained using the MP2/6-31+G(d) level of theory combined with the IEFPCM solvation model. The most remarkable feature of the *cis*/*trans*-rotamerisation is that the amide nitrogen in AcProOH and AcHypOH adopts a tetrahedral geometry in the transition state. We have also shown that the MP2 calculations combined with implicit solvation models are reasonably accurate in reproducing NMR measured populations of four different conformations of either AcProOH or AcHypOH in different solvents, whereas HF and DFT B3LYP calculations were significantly less accurate. From the experimental NMR measurements of various Pro containing peptides, the relative stability of the *cis*- and *trans*-rotamers and the free energy of activation for the *cis*/*trans*-rotamerisation showed a significant dependence on the solvent properties and on the nature of the substituent preceding the Pro residue.

Acknowledgment. We thank UCL for the provision of the NMR and computational facilities and EPSRC for financial support. We are grateful to Jeremy Yates, Clare Gryce, and Brian Alston from the Legion Research Computing team for their help with our QM and MD calculations.

Supporting Information Available: Further results of NMR measurements and QM calculations. This material is available free of charge via the Internet at http://pubs.acs.org.

References and Notes

(1) Watanabe, K.; Masuda, T.; Ohashi, H.; Mihara, H.; Suzuki, Y. *Eur. J. Biochem.* **1994**, *226*, 277.
(2) Brandl, C.; Deber, C. M. *Proc. Natl. Acad. Sci. U.S.A.* **1986**, *83*, 917.
(3) Barlow, D. J.; Thornton, J. M. *J. Mol. Biol.* **1988**, *201*, 601.
(4) Wedemeyer, W. J.; Welker, E.; Scheraga, H. A. *Biochemistry* **2002**, *41*, 14637.
(5) Ramachandran, G. N.; Mitra, A. K. *J. Mol. Biol.* **1976**, *107* 85.
(6) Dorman, D. E.; Bovey, F. A. *J. Org. Chem.* **1973**, *38*, 2379.
(7) Siemion, I. Z.; Wieland, T.; Pook, K.-H. *Angew. Chem.* **1975**, *87*, 702.
(8) Mizuno, K.; Hayashi, T.; Peyton, D. H.; Bachinger, H. P. *J. Biol. Chem.* **2004**, *279*, 38072.
(9) Shoulders, M. D.; Hodges, J. A.; Raines, R. T. *J. Am. Chem. Soc.* **2006**, *128*, 8112.
(10) Sonntag, L.-S.; Schweizer, S.; Ochsenfeld, C.; Wennemers, H. *J. Am. Chem. Soc.* **2006**, *128*, 14697.
(11) Altona, C.; Sundaralingam, M. *J. Am. Chem. Soc.* **1972**, *94*, 8205.
(12) Haasnoot, C. A. G.; DeLeeuw, F. A. A. M.; DeLeew, H. P. M.; Altona, C. *Biopolymers* **1981**, *20*, 1211.
(13) Aliev, A. E.; Courtier-Murias, D. *J. Phys. Chem. B* **2007**, *111*, 14034.
(14) Schmidt, J. M.; Brüschweiler, R.; Ernst, R. R.; Dunbrack, R. L.; Joseph, D.; Karplus, M. *J. Am. Chem. Soc.* **1993**, *115*, 8747.
(15) Brunne, R. M.; van Gunsteren, W. F.; Brüschweiler, R.; Ernst, R. R. *J. Am. Chem. Soc.* **1993**, *115*, 4764.
(16) Fischer, S.; Dunbrack, R. L., Jr.; Karplus, M. *J. Am. Chem. Soc.* **1994**, *116*, 11931.
(17) Kang, Y. K. *J. Phys. Chem.* **1996**, *100*, 11589.
(18) Jhon, J. S.; Kang, Y. K. *J. Phys. Chem. A* **1999**, *103*, 5436.
(19) Kang, Y. K.; Choi, H. Y. *Biophys. Chem.* **2004**, *111*, 135.
(20) Kang, Y. K. *J. Phys. Chem. B* **2004**, *108*, 5463.
(21) Song, I. K.; Kang, Y. K. *J. Phys. Chem. B* **2005**, *109*, 16982.
(22) Kang, Y. K. *J. Phys. Chem. B* **2006**, *110*, 21338.
(23) Kang, Y. K. *J. Phys. Chem. B* **2007**, *111*, 10550.
(24) Improta, R.; Benzi, C.; Barone, V. *J. Am. Chem. Soc.* **2001**, *123*, 12568.
(25) Benzi, C.; Improta, R.; Scalmani, G.; Barone, V. *J. Comput. Chem.* **2001**, *123*, 12568.
(26) Kapitán, J.; Baumruk, V.; Kopecký, V.; Pohl, R.; Bouř, P. *J. Am. Chem. Soc.* **2006**, *128*, 13451.
(27) Budíšínský, M.; Daněček, P.; Bednárová, L.; Kapitán, J.; Baumruk, V.; Bouř, P. *J. Phys. Chem. A* **2008**, *112*, 8633.
(28) Pálfi, V. K.; Perczel, A. *J. Comput. Chem.* **2008**, *29*, 1374.
(29) Yonezawa, Y.; Nakata, K.; Sakakura, K.; Takada, T.; Nakamura, H. *J. Am. Chem. Soc.* **2009**, *131*, 4535.
(30) *gNMR*, Version 5.0.6, NMR Simulation Program, Budzelaar PHM, 2006.

(31) Press, W. H.; Flannery, B. P.; Teukolsky, S. A. *Numerical Recipes in FORTRAN: the Art of Scientific Computing*, Cambridge University Press, 1992.

(32) Haasnoot, C. A. G.; DeLeeuw, F. A. A. M.; Altona, C. *Tetrahedron* **1980**, *36*, 2783.

(33) Frisch, M. J.; Trucks, G. W.; Schlegel, H. B.; Scuseria, G. E.; Robb, M. A.; Cheeseman, J. R.; Montgomery Jr., J. A.; Vreven, T.; Kudin, K. N.; Burant, J. C.; Millam, J. M.; Iyengar, S. S.; Tomasi, J.; Barone, V.; Mennucci, B.; Cossi, M.; Scalmani, G.; Rega, N.; Petersson, G. A.; Nakatsuji, H.; Hada, M.; Ehara, M.; Toyota, K.; Fukuda, R.; Hasegawa, J.; Ishida, M.; Nakajima, T.; Honda, Y.; Kitao, O.; Nakai, H.; Klene, M.; Li, X.; Knox, J. E.; Hratchian, H. P.; Cross, J. B.; Adamo, C.; Jaramillo, J.; Gomperts, R.; Stratmann, R. E.; Yazyev, O.; Austin, A. J.; Cammi, R.; Pomelli, C.; Ochterski, J. W.; Ayala, P. Y.; Morokuma, K.; Voth, G. A.; Salvador, P.; Dannenberg, J. J.; Zakrzewski, V. G.; Dapprich, S.; Daniels, A. D.; Strain, M. C.; Farkas, O.; Malick, D. K.; Rabuck, A. D.; Raghavachari, K.; Foresman, J. B.; Ortiz, J. V.; Cui, Q.; Baboul, A. G.; Clifford, S.; Cioslowski, J.; Stefanov, B. B.; Liu, G.; Liashenko, A.; Piskorz, P.; Komaromi, I.; Martin, R. L.; Fox, D. J.; Keith, T.; Al-Laham, M. A.; Peng, C. Y.; Nanayakkara, A.; Challacombe, M.; Gill, P. M. W.; Johnson, B.; Chen, W.; Wong, M. W.; Gonzalez, C.; Pople, J. A. *Gaussian 03*, Revision D.02; Gaussian Inc.: Wallingford, CT, 2004.

(34) (a) Cances, E.; Mennucci, B. *J. Math. Chem.* **1998**, *23*, 309. (b) Cances, E.; Mennucci, B.; Tomasi, J. *J. Chem. Phys.* **1997**, *107*, 3032. (c) Mennucci, B.; Cances, E.; Mennucci, B.; Tomasi, J. *J. Phys. Chem. B* **1997**, *101*, 10506.

(35) Barone, V.; Cossi, M. *J. Phys. Chem. B* **1998**, *102*, 1995.

(36) Westhof, G.; Sundaralingam, M. *J. Am. Chem. Soc.* **1983**, *105*, 970.

(37) Delaney, N. G.; Madison, V. *J. Am. Chem. Soc.* **1982**, *104*, 6635.

(38) Madison, V.; Kopple, K. D. *J. Am. Chem. Soc.* **1980**, *102*, 4855.

(39) Shanan-Atidi, H.; Bar-Eli, K. H. *J. Phys. Chem.* **1970**, *74*, 961.

(40) Scheiner, S.; Kern, C. W. *J. Am. Chem. Soc.* **1977**, *99*, 7042.

(41) Kessler, H. *Angew. Chem.* **1970**, *82*, 237.

(42) Murphy, R. B.; Beach, M. D.; Friesner, R. A.; Ringnalda, M. N. *J. Chem. Phys.* **1995**, *103*, 1481.

(43) Friesner, R. A. *Proc. Natl. Acad. Sci. U.S.A.* **2005**, *102*, 6648.

(44) Grimme, S. *Angew. Chem., Int. Ed.* **2006**, *45*, 4460.

(45) Grimme, S.; Mück-Lichtenfeld, C. *Chirality* **2008**, *20*, 1009.

(46) Echenique, P.; Alonso, J. L. *J. Comput. Chem.* **2008**, *29*, 1408.

(47) Peng, C.; Ayala, P. Y.; Schlegel, H. B.; Frisch, M. J. *J. Comput. Chem.* **1996**, *17*, 49.

JP906006W